Deep long-period earthquakes at Akutan Volcano are more directly related to magmatic processes than volcano-tectonic earthquakes

Zilin Song[1], Yen Joe Tan[2], and Diana C. Roman[3]

[1]Chinese University of Hong Kong
[2]The Chinese University of Hong Kong
[3]Carnegie Institution of Washington

December 7, 2022

Abstract

Both volcano-tectonic (VTs) and deep long-period earthquakes (DLPs) have been documented at Akutan Volcano, Alaska and may reflect different active processes. In this study, we perform high-resolution earthquake detection, classification, and relocation using seismic data from 2005-2017 to investigate their relationship with underlying magmatic processes. We find that the 2,787 VTs and 787 DLPs are concentrated above and below the shallow magma reservoir respectively. The DLPs' low-frequency content is likely a source instead of path effect considering its uniformity across stations. Both VT and DLP swarms occur preferentially during inflation episodes with no clear migration. However, the largest VT swarms occur during non-inflating periods, and only VT swarms contain repeating events. Therefore, we conclude that the VTs represent fault rupture triggered by magma/fluid movement or larger earthquakes, while the DLPs are directly related to unsteady magma movement through a complex pathway or represent slow fault ruptures triggered by magma movement.

Deep long-period earthquakes at Akutan Volcano are more directly related to magmatic processes than volcano-tectonic earthquakes

Zilin SONG[1], Yen Joe TAN[1], Diana C. Roman[2]

[1]Earth and Atmospheric Sciences, The Chinese University of Hong Kong, Hong Kong, China
[2]Earth and Planets Laboratory, Carnegie Institution for Science, Washington, DC 20015, USA

Key Points:

- Akutan deep long-period earthquakes are likely due to source instead of just path or station site effects.
- Both deep long-period and volcano-tectonic earthquake swarms occur preferentially during inflation episodes with no clear migration.
- Moment release of deep long-period earthquake swarms is more strongly correlated with inflation episodes than volcano-tectonic earthquakes.

Corresponding author: Yen Joe TAN, `yjtan@cuhk.edu.hk`

Abstract

Both volcano-tectonic (VTs) and deep long-period earthquakes (DLPs) have been documented at Akutan Volcano, Alaska and may reflect different active processes. In this study, we perform high-resolution earthquake detection, classification, and relocation using seismic data from 2005-2017 to investigate their relationship with underlying magmatic processes. We find that the 2,787 VTs and 787 DLPs are concentrated above and below the shallow magma reservoir respectively. The DLPs' low-frequency content is likely a source instead of path effect considering its uniformity across stations. Both VT and DLP swarms occur preferentially during inflation episodes with no clear migration. However, the largest VT swarms occur during non-inflating periods, and only VT swarms contain repeating events. Therefore, we conclude that the VTs represent fault rupture triggered by magma/fluid movement or larger earthquakes, while the DLPs are directly related to unsteady magma movement through a complex pathway or represent slow fault ruptures triggered by magma movement.

Plain Language Summary

Volcano eruption forecasting is a challenging task that often requires the deciphering of processes underlying observed signs of volcanic unrest. As seismometers become common monitoring sensors on volcanoes, the recorded ground motion is valuable for scientists to study eruption precursors. Earthquakes are commonly observed and generally inferred to be associated with stress perturbations in the shallow crust. However, earthquakes with predominantly lower-frequency energy are sometimes observed at depth and their origin is enigmatic. In this paper, we use the existing catalog of earthquakes at Akutan Volcano in Alaska between 2005-2017 as templates to successfully detect more earthquakes before locating them with higher precision. We find that the earthquakes tend to occur in bursts and during times when surface inflation was also detected due to ascending magma. However, only the sizes of the earthquakes with lower-frequency energy are strongly correlated with surface inflation. Their waveform characteristics also suggest their underlying source mechanism is different from regular earthquakes. Therefore, we conclude that these lower-frequency earthquakes are related to unsteady magma movement through a complex pathway unlike regular earthquakes which represent sudden fault movements.

1 Introduction

Seismometers are the most commonly deployed monitoring sensors on volcanoes (Saccorotti & Lokmer, 2021) as exemplified by the seismic networks maintained by the Hawaiian (Nakata & Okubo, 2010) and Alaska (Power et al., 2013) volcano observatories. Over the years, development in volcano seismology has given rise to several successes in eruption forecasting. Recent examples include the 1991 Pinatubo (Harlow et al., 1996) and 2000 Hekla eruptions (Einarsson, 2018) which were successfully forecasted based on precursory increases in seismicity rate. However, seismic anomalies prior to eruptions are not always observed, limiting our forecasting ability. For instance, only 30% of recent eruptions among Alaskan volcanoes have statistically significant precursory increase in seismicity rate (Pesicek et al., 2018). Cameron et al. (2018) also found that between 1989-2017, Alaska Volcano Observatory's (AVO) forecasting success rate for certain types of volcanoes e.g. those with short repose time (<15 years) or small eruption size (Volcanic Explosivity Index of 2 or less) is <20%. Therefore, further advances in our understanding of how seismic activity evolves through eruption cycles and relate to various volcanic and magmatic processes at different volcanoes are crucial for improving our ability to forecast eruptions (Thelen et al., 2022).

Earthquake occurrence are often clustered in space and time. The most common clustering are mainshock-aftershock sequences where the largest magnitude earthquake (i.e. mainshock) is followed by decaying numbers of smaller earthquakes nearby (i.e. aftershocks), with the magnitude difference between the mainshock and the largest aftershock being ~ 1.2 on average (Båth, 1965). Mainshock-aftershock sequences are generally thought to reflect a cascade of inter-event stress triggering (Marsan & Lengliné, 2008). Another type of clustering, where a burst of seismic activity is not associated with a clear mainshock, is commonly termed swarms (Mogi, 1963; Roland & McGuire, 2009). Swarms occurring on plate boundary fault systems are often inferred to indicate fluid diffusion in heterogeneous structures (Nishikawa & Ide, 2017; Ross & Cochran, 2021) or aseismic slip in low coupling regions (Nishikawa & Ide, 2018; Peng et al., 2021). In comparison, swarms in volcanic or geothermal regions are often inferred to be related to migration of magma (Power et al., 1998; Hensch et al., 2008) or hydrothermal fluids (Shelly et al., 2013), though these interpretations can be non-unique. In addition, while the proportion of swarms versus mainshock-aftershock sequences is thought to be higher in volcanic compared to non-volcanic regions (Benoit & McNutt, 1996), this is still under debate (Vidale et al., 2006; Traversa & Grasso, 2010; Garza-Giron et al., 2018). Therefore, it remains challenging to interpret the physical mechanism underlying bursts of seismic activity at volcanic regions.

Earthquakes recorded at volcanic regions that are rich in high-frequency content are usually referred to as volcano-tectonic events (VTs). VTs are commonly observed in the shallow crust (e.g. Matoza et al. (2014)) and considered to be related to stress perturbation from processes such as shear failures in volcanic edifice (Chouet & Matoza, 2013) or dike propagation (Roman & Cashman, 2006). In contrast, earthquakes that predominantly radiate low-frequency (1-5 Hz) energy are sometimes found at mid- to lower-crustal depths (Power et al., 2004; Kurihara & Obara, 2021) and are known as deep long-period events (DLPs). DLPs are characterized by emergent phase arrivals which make them hard to detect using traditional earthquake detection methods (Pitt, 2002). Therefore, even though it has been observed that eruptions, steam emission and summit inflation are sometimes preceded by DLPs which points to their potential as eruption precursors (R. A. White, 1996; Power et al., 2013), these events are not well studied. Various source mechanisms for DLPs have been proposed, and generally fall into two categories: 1) DLPs are generated near stalled magma e.g. due to thermal stress from magma cooling (Aso & Tsai, 2014) or volatile release from second boiling (Wech et al., 2020); 2) DLPs are generated where there is unsteady fluid movement e.g. due to intermittent magma flow (Ukawa & Ohtake, 1987), melt degassing (Melnik et al., 2020) or resonance in fluid-filled cracks (Bean et al., 2014). Nevertheless, sometimes it is difficult to even ascertain whether the observed waveform characteristics of DLPs are due to source or path effects (Saccorotti & Lokmer, 2021). Deciphering the physical processes underlying DLPs will improve their utility for volcano monitoring purposes.

Akutan Volcano is one of the most active volcanoes in the Aleutian Arc with at least 27 eruptive episodes reported since 1790 (Miller et al., 1998; Lu & Dzurisin, 2014). A network of 14 seismometers has been deployed around the volcano since 1996 and both VTs and DLPs have been documented (Power et al., 2004). In addition, based on both Interferometric Synthetic Aperture Radar (InSAR) (Lu et al., 2000; Wang et al., 2018) and local Global Positioning System (GPS) (Ji & Herring, 2011; Ji et al., 2017) observations, a magma reservoir is inferred to be located at $\sim$8 km depth with inflation episodes every 2-3 years between 2002-2017. Therefore, Akutan Volcano is a promising site to investigate the characteristics of DLPs and VTs and their relationship to magmatic processes. In this paper, we analyze 12 years of continuous waveform data at Akutan Volcano to detect and locate VTs and DLPs using cross-correlation-based template matching (Gibbons & Ringdal, 2006) and double-difference relocation (Waldhauser & Ellsworth, 2000). We then characterize their spatiotemporal clustering properties and how their activities relate with the inflation episodes, as well as investigate the underlying cause for the waveform characteristics of DLPs.

2 Matched filter detection, magnitude estimation, and relocation

Between November 2005 and December 2017, continuous waveform data from 14 stations (Fig. 1a) are available from the Incorporated Research Institution for Seismology Data Management Center (IRIS DMC), whereas between 2002-2005, 1-minute event waveforms are available (Alaska Volcano Observatory/USGS, 1988). Therefore, we obtain waveforms of 1785 events from 2002-2017 in the unified catalog of earthquakes produced by the AVO (Power et al., 2019) falling in the region of [(53.9°, -166.5°), (54.5°, -166.5°), (53.9°, -165.9°), (54.5°, -165.9°)] (Fig. 1). All waveforms are resampled to 50 Hz and bandpass filtered 1-15 Hz, and only those with signal-to-noise ratio (SNR) above 2 are retained for further analysis.

We apply EQcorrscan, an open-source python package, to perform matched filter detection (Chamberlain et al., 2017). By cross-correlating waveforms of template events with continuous waveforms across the seismic network, detections are declared when the sum of normalized cross-correlations (NCC) exceeds a certain threshold. We use 1,510 events with distinct (SNR>2) P arrival on the vertical channel or S arrival on the horizontal channel of more than 4 stations as templates. Template waveforms start from 1s before P/S arrivals and have lengths of 7 s. Each template is used to scan through continuous data from 2005-2017 (Fig. S1). To improve the stability of the detection process, we split the continuous waveforms into hourly segments with 30 s overlaps and remove traces with excessive gaps or spikes before the template matching process (Warren-Smith et al., 2017).

We use 10 times median absolute deviation (MAD) as a conservative threshold for declaring a detection following Hotovec-Ellis et al. (2018). Since the matched filter detection method mainly detects events with similar waveforms as the templates, our detections can be limited by the available initial catalog of templates. To quantify this effect, we check whether each of our 1278 templates between 2005-2017 was detected from continuous waveforms by any other templates using EQcorrscan. We find that 99.61% of the templates were successfully detected by another template which suggests that the method can detect unique events reasonably well. We further manually inspect new detections' waveforms and remove detections with average network NCC that is less than 0.4 to remove false detections. Finally, for detections with origin time difference of less than 2 s, the ones with the lowest NCC values are removed to avoid duplicate (van Wijk et al., 2021). We end up with 2,077 newly-detected events.

For newly-detected events, we estimate their local magnitudes as follow:

$$M_{detection} = M_{template} + c * log(\alpha) \tag{1}$$

where α is the amplitude ratio between detected and template events while c is a constant that scales the amplitude-magnitude difference and is approximately 1 (Fig. S2) (Schaff, 2008; Shelly et al., 2016). We measure α using principal component analysis on 7s long waveforms and use the median α value from paired waveforms across all the available stations. The magnitude of completeness (M_c) improved from M_L 0.1 to M_L -0.3 (Fig. S3) when estimated using the maximum curvature method (Wiemer & Wyss, 2000).

We then relocate both the catalog (Power et al., 2019) and newly detected events using the HypoDD double-difference method (Waldhauser & Ellsworth, 2000). Newly detected events are assumed to be co-located with their templates as initial input to HypoDD. We calculate pick-derived differential arrival times for all event pairs within 10 km of each other with at least 6 observations. For event pairs with distance less than 5 km, we derive cross-correlation-derived differential arrival times at each station when NCC value of the waveforms is larger than 0.7. The window begins 0.5 s before and continue for 1.5 s and 2 s after the P and S-wave arrivals, respectively. We successfully relocate 3,144 events using a 3D velocity model from Syracuse et al. (2015) between November 2005 and December 2017 (Fig. 1c). We then perform bootstrapping by repeatedly relocating 100 random events using singular value decomposition mode to estimate their location uncertainties (Waldhauser & Ellsworth, 2000). On average, we find that the relative horizontal and vertical location uncertainties are 0.75 km and 1.07 km respectively.

3 Earthquake classification

The long-period (LP) and VT events in the AVO catalog have been manually classified (Power et al., 2019), but manual classifications are subjective and can be inconsistent (Matoza et al., 2014). Therefore, we reclassify all events systematically using the frequency index (FI) following Buurman and West (2010):

$$FI = \log_{10}\left(\overline{A}_{upper}/\overline{A}_{lower}\right) \tag{2}$$

where $\overline{A}_{upper}$ and $\overline{A}_{lower}$ represent mean spectral amplitudes in the higher and lower frequency bands respectively. For each event, we calculate the power spectral density spectrum of its vertical component seismograms with a 7 s time window starting from 1 s before the P picks, after correcting for instrument response. When P pick is unavailable from the catalog, we use the predicted arrival time derived from the event location and 1-D velocity model (Power et al., 2019). We first calculate FI at each station using 10-15 Hz and 1-5 Hz as the A_{upper} and A_{lower} respectively, since we find that these frequency bands allow the FI to most effectively differentiate the VTs and DLPs (Fig. S4). The median FI across all available stations is then assigned to each event as their final FI value.

Figure 1b shows the FI distribution of earthquakes in the AVO catalog, color-coded by their manual labels (Power et al., 2019). There is a clear bimodal distribution and near the boundary, manual labels can be inconsistent i.e. events with the same FI values can have different labels. We select FI of -1.6 as the classification boundary, hence 259 events with FI lower than -1.6 are classified as LP while the remaining events are classified as VT. Newly detected events are classified into the same category as their templates. Overall, 561 newly detected events are LPs which is 2 times more than the number of LP templates. In comparison, 1,516 newly detected events are VTs which is similar to the number of VT templates. The larger number of new detection relative to the available templates for LP events may reflect AVO's current event detection system being less well-optimized for detecting LP events.

Combined with earthquake spatial distributions (Fig. 1c), we observe that 1) most VTs are located beneath the caldera and above the inferred magma reservoir (DeGrandpre et al., 2017); 2) there are some VTs located to the west of the caldera that extend down to 30 km depth; 3) most LPs are located below the inferred magma reservoir in a region with low P wave velocity (Syracuse et al., 2015). We refer to these LPs below the shallow magma reservoir as DLPs.

4 Earthquake clusters and moment release

We cluster the LP and VT events above M_c separately following Mogi (1963)'s algorithm which takes into account 1) the total number of events in a sequence (E_T), and 2) the empirical relation between maximum number of daily events (N_d) and duration of sequence in days (T):

$$N_d > 2 \times \sqrt{T} \tag{3}$$

We use E_T of 10 as the minimum threshold to define a cluster and iterate through T values from 0.5 to 5. For each cluster, we calculate the distance between each clustered earthquake and the largest one. Events located further than 3 times standard deviation from the largest earthquake are regarded as outliers and removed. To improve clustering results, absolute locations are also used for earthquakes that are not successfully relocated (Fig. S5). We finally obtain 8 DLP and 34 VT clusters (Fig. 2c) and further classify each cluster as a swarm when 1) the magnitude difference between the largest magnitude event and the following second largest events is less than 1, and 2) the occurrence time of the largest event is near/after the middle of the sequence. We find that all DLP and VT clusters fulfill these criteria and are classified as swarms (Fig. S6). There are no mainshock-aftershock sequences detected.

For each swarm, we estimate its cumulative moment release. The seismic moment (M_0) of each event is calculated as

$$M_0 = 10^{1.5*M_w+9.105} \tag{4}$$

where M_w represents an earthquake's moment magnitude. We obtain each event's M_w by converting their M_L following $M_w = M_L$ for $M_L > 3$ events (Kanamori & Brodsky, 2004) and $M_w = 2/3*M_L+1$ for $M_L \leq 3$ events (Munafò et al., 2016), which accounts for the expected change in scaling between M_L and M_w for smaller earthquakes (Deichmann, 2017). Cumulative moment release of a swarm is the sum of M_0 for all the involved earthquakes.

5 Discussion

5.1 Dominant frequency content of DLPs

As the VTs and DLPs predominantly located in different regions (Fig. 1c), the difference in their dominant frequency content could be a result of differences in wave propagation path with different attenuation effect. Firstly, we investigate whether the lower frequency content of DLPs can be a path effect due to the overlying low velocity regions (Fig. S7a) with the presence of melt or extensive fracturing (Coté et al., 2010; Bean et al., 2014; Clarke et al., 2021). We calculate the FI values of DLPs recorded at the MTBL station which is located ∼50 km west of Akutan Volcano (Fig. 1a). We find that their FI values remain low (Fig. 3a) and similar to the FI values measured using waveforms recorded on the local stations (Fig. 1b). In comparison, deep VTs located a few kilometers west of the DLP zone recorded on the MTBL station all have higher FI values (Fig. 3a-b) despite having similar travel paths (Fig. S7a). Therefore, we conclude that the lower frequency content of DLPs at Akutan Volcano is not only a path effect due to the overlying structure.

Subsequently, we investigate whether the lower frequency content of DLPs is a path effect due to attenuation in their source region (Fig. S7b). In this case, there should not be any VT events in the DLP source region. However, while they do not occur in large numbers, we manage to identify ∼60 deep VT events within the DLP source region (Fig. 3b-c, S8). Time differences between P and S arrivals of the deep VTs are similar to those of deep LPs and significantly larger than those of shallow VTs, indicating that these deep VTs are not mislocated (Fig. 3c, S8). Hence, the lower frequency content of DLPs at Akutan Volcano is unlikely to be only a path effect due to attenuation in their source region. Therefore, we conclude that the lower frequency content of DLPs at Akutan Volcano is most probably a source effect, though we cannot completely rule out the possibility of kilometer-scale structural heterogeneity with highly variable attenuation effect around the DLP source region (Fig. S7c).

5.2 How VT and DLP swarms relate to inflation episodes

Earthquake swarms have been found to sometimes coincide with volcanic inflation e.g. (Ji et al., 2017). Swarms are considered more likely to occur in volcanic regions than mainshock-aftershock sequences due to the presence of hydrothermal fluids or viscous flow, which can reduce rocks' elastic moduli and hence earthquake aftershock productivity (Garza-Giron et al., 2018). This is consistent with our findings at Akutan where all the clustered VTs and DLPs are swarms instead of mainshock-aftershocks. To investigate how VT and DLP relate to magma movements, we analyze temporal correlations between identified swarms and magma inflation at Akutan. Based on GPS measurement from November 2005 to December 2017, we manually identify 4 inflation episodes, each lasting 5-14 months (Fig. 2), when the inferred Mogi source exhibits a significant volume increase (Xue et al., 2020). In total, the inflation episodes span 39 months out of the 145 months that our study period encompasses. We find that 3 (73 DLPs) out of the 8 DLP swarms (179 DLPs) and 13 (225 VTs) out of the 34 VT swarms (541 VTs) occurred during an inflation episode. That means the rate of DLP and VT swarms are 0.92 and 4.00 per year (22.46 DLPs/year and 69.23 VTs/year) respectively during the inflating periods, which is almost twice the rate of 0.57 and 2.38 per year (12.00 DLPs/year and 35.77 VTs/year) during the non-inflating periods (Fig. 2a). Therefore, both DLP and VT occurrence are strongly correlated with magma inflation. This finding is relatively robust, since we find that both DLP and VT swarms rates during inflation episodes remain higher than during non-inflating periods even when we do not cluster earthquakes or use E_T of 5 or 15 instead during the clustering process (Fig. S9-10, Table S1). We also find that the proportions of VT and DLP swarms corresponding to surface inflation are both 0.38 even though they are located in different regions (Fig. 1c). In addition, neither VT nor DLP swarms show clear migration from depth with time (Fig. 2c, Fig. S6), which is similar to observations at Makushin Volcano (Lanza et al., 2022). Such event migrations at Akutan should have been resolvable since half of all identified swarms span at least 5 km spatially (Fig. S6) compared to the earthquake location uncertainty of only $\sim$1 km.

Previous research suggests that cumulative moment release of proximal volcanic earthquake swarms in a single swarm can be used as a proxy for intruded magma volume (R. White & McCausland, 2016). If this relationship holds for Akutan Volcano, swarms occurring during inflation episodes should have larger cumulative moment releases compared to those occurring during non-inflation periods. We find that the two largest DLP swarms in terms of cumulative moment releases indeed occurred during an inflation episode (Fig. 2d). The third DLP swarm that occurred during an inflation episode in 2016 have comparable cumulative moment releases with the two largest DLP swarms that occurred during non-inflation periods. In comparison, the largest VT swarms in terms of cumulative moment releases do not coincide with inflation episodes (Fig. 2d). We also estimate the moment release rates of DLP and VT swarms during inflation and non-inflation periods (Fig. 2b). We find that the moment release rates of DLP swarms during inflation periods is 3.88×10^{13} N·m/year, which is significantly larger than 2.26×10^{12} N·m/year during non-inflation periods. Comparatively, the moment release of VT swarms in inflation periods (1.21×10^{13} N·m/year) is only slightly higher than that in non-inflation periods (1.03×10^{13} N·m/year). This pattern remains consistent when we use either all the events with magnitude above magnitude completeness or E_T of 5 and 15 instead during the clustering process (Table S2, Fig. S10). Therefore, it appears that although both DLP and VT swarms occur preferentially during inflation episodes, the moment release of DLP swarms is more strongly correlated with magma inflation compared to VT swarms.

5.3 Physical process underlying VT and DLP swarms

Swarms of VT are commonly inferred to be related to physical processes like dike propagation (Roman & Cashman, 2006), fluid diffusion (Yukutake et al., 2011), and aseismic slip (Yukutake et al., 2022) based on observations of vertical alignment in earthquake distributions (Roman & Cashman, 2006), earthquake migration speed that gives reasonable diffusivity/permeability estimates (Yukutake et al., 2011), and detections of repeating earthquakes (Yukutake et al., 2022). In comparison, DLP swarms have been associated with magma transport based on their low-frequency energy content, non-double-couple source moment tensor (Oikawa et al., 2019), and migration path that co-locates with estimated magma movement path (Kurihara et al., 2019) or stalled magma at depth based on observations of stationary, repeating DLPs that correlate with gas emissions (Wech et al., 2020).

At Akutan, the VT swarms do not delineate clear planar structures nor show clear migration patterns. Therefore, they are unlikely to represent dike propagation. The VT events are mostly located within regions with high V_p (Fig. 1c) hence regions without pervasive fluids (Yukutake et al., 2015). However, due to the limited spatial resolution of the tomography study (Syracuse et al., 2015), it remains possible that these swarms were triggered by small-scale fluid diffusion (Igarashi et al., 2003; Hatch et al., 2020). In addition, we have identified "repeating" events with highly similar (NCC>0.9) waveforms (Fig. S11) within these swarms, though we could not verify that their rupture areas indeed overlap. Considering that the VT swarms are more likely to occur during inflation episodes, they might reflect fault asperities that were driven to failure due to stress loading from the underlying inflating magma reservoir. However, since many VT swarms, including the ones with the largest cumulative moment release, occur during non-inflation periods, they are likely also linked to other non-magmatic processes e.g. fluid diffusion (Farrell et al., 2009) or triggering by nearby or far-field large earthquakes (Peng et al., 2021).

Repeating DLPs are usually interpreted to reflect a repeating, non-destructive source process occurring at the same location, such as rapid pressure changes due to magmatic gas passing through cracks (Brill & Waite, 2019; Wech et al., 2020) or resonance of a fixed geometry fluid-filled crack (Okubo & Wolfe, 2008). However, out of the ~600 DLPs at Akutan, we only find one pair with NCC value above 0.9 and these two events have FI of -1.7 which is close to the boundary of -1.6 that we used to separate LP and VT events. Therefore, we conclude that DLPs at Akutan do not reflect a stationary, repeating source process. Considering the DLP swarms, especially the ones with the largest cumulative moment release, are strongly correlated with inflation episodes and their low-frequency content is likely a source effect, we infer that DLPs at Akutan are either directly related to unsteady magma movement through a complex pathway (Kurihara et al., 2019) or represent slow fault ruptures triggered by magma movement (Bean et al., 2014). In this case, the lack of DLP swarms during certain inflation episodes (Fig. 2b) could reflect aseismic magma movement e.g. magma flow that are too slow to radiate detectable seismic energy (Gualandi et al., 2017). DLP swarms occurring outside of inflation episodes with smaller cumulative moment release (Fig. 2c) could instead represent magma influxes that are too small or too deep to generate surface deformation signal detectable by the existing GPS network.

6 Conclusions

In conclusion, we detected 2,077 new events at Akutan Volcano by applying template matching on continuous data from 2005-2017. We then systematically classified all events into 2,787 VTs and 767 LPs based on their frequency index. After waveform-based double difference relocation, we find that the VTs and DLPs are primarily distributed above and below the shallow magma reservoir (10 km depth) respectively. The low-frequency content of DLPs is relatively uniform across the seismic network hence is likely a source instead of path or site effect. After clustering both VTs and DLPs based on their interevent time, distance and magnitude, we find that they both only occur as swarms instead of mainshock-aftershock sequences. In addition, while they occur asynchronously with no clear depth migration, both DLP and VT swarms occur preferentially with greater moment release during inflation episodes. However, the largest VT swarms in terms of cumulative moment releases do not coincide with inflation episodes and only VT swarms contain repeating events. Therefore, we infer that the VT swarms likely reflect fault slips triggered by magma inflation, fluid diffusion or larger earthquakes. In contrast, we infer that the DLP swarms are either directly related to unsteady magma movement through a complex pathway or represent slow fault ruptures triggered by magma movement.

Open Research

A unified catalog of earthquake hypocenters and magnitudes at Alaska volcanoes during 1989-2018 from Power et al. (2019) is used for this research, which is available at https://doi.org/10.3133/sir20195037. Using IRIS Data Services, waveforms and related metadata from Alaska Volcano Observatory and Alaska Regional Network can be accessed at https://doi.org/10.7914/SN/AK and https://doi.org/10.7914/SN/AV.

Acknowledgments

Z. Song and Y.J. Tan are supported by Tan's start-up fund (Grant Number 4053512) and the Direct Grant for Research (Grant Number 4053483) from the Chinese University of Hong Kong, Hong Kong RGC General Research Fund Grant Number 14300422, and the Croucher Tak Wah Mak Innovation Award.

References

Alaska Volcano Observatory/USGS. (1988). *Alaska volcano observatory.* International Federation of Digital Seismograph Networks. Retrieved from `https://www.fdsn.org/networks/detail/AV/` doi: 10.7914/SN/AV

Aso, N., & Tsai, V. C. (2014). Cooling magma model for deep volcanic long-period earthquakes [Journal Article]. *Journal of Geophysical Research: Solid Earth*, *119*(11), 8442-8456. Retrieved from `https://agupubs.onlinelibrary.wiley.com/doi/abs/10.1002/2014JB011180` doi: https://doi.org/10.1002/2014JB011180

Bean, C. J., De Barros, L., Lokmer, I., Métaxian, J.-P., O' Brien, G., & Murphy, S. (2014). Long-period seismicity in the shallow volcanic edifice formed from slow-rupture earthquakes [Journal Article]. *Nature Geoscience*, *7*(1), 71-75. Retrieved from `https://doi.org/10.1038/ngeo2027` doi: 10.1038/ngeo2027

Benoit, J. P., & McNutt, S. R. (1996). *Global volcanic earthquake swarm database 1979-1989* (Report No. 96-69). Retrieved from `http://pubs.er.usgs.gov/publication/ofr9669` doi: 10.3133/ofr9669

Brill, K. A., & Waite, G. P. (2019). Characteristics of repeating long-period seismic events at fuego volcano, january 2012 [Journal Article]. *Journal of Geophysical Research: Solid Earth*, *124*(8), 8644-8659. Retrieved from `https://doi.org/10.1029/2019JB017902` doi: https://doi.org/10.1029/2019JB017902

Buurman, H., & West, M. (2010). Seismic precursors to volcanic explosions during the 2006 eruption of augustine volcano [Journal Article]. *The 2006 Eruption of Augustine Volcano, Alaska*, *1769*.

Båth, M. (1965). Lateral inhomogeneities of the upper mantle [Journal Article]. *Tectonophysics*, *2*(6), 483-514.

Cameron, C. E., Prejean, S. G., Coombs, M. L., Wallace, K. L., Power, J. A., & Roman, D. C. (2018). Alaska volcano observatory alert and forecasting timeliness: 1989–2017 [Journal Article]. *Frontiers in Earth Science*, *6*. Retrieved from `https://www.frontiersin.org/article/10.3389/feart.2018.00086` doi: 10.3389/feart.2018.00086

Chamberlain, C. J., Hopp, C. J., Boese, C. M., Warren-Smith, E., Chambers, D., Chu, S. X., … Townend, J. (2017). Eqcorrscan: Repeating and near-repeating earthquake detection and analysis in python [Journal Article]. *Seismological Research Letters*, *89*(1), 173-181. Retrieved from `https://doi.org/10.1785/0220170151` doi: 10.1785/0220170151

Chouet, B. A., & Matoza, R. S. (2013). A multi-decadal view of seismic methods for detecting precursors of magma movement and eruption [Journal Article]. *Journal of Volcanology and Geothermal Research*, *252*, 108-175. Retrieved from `https://www.sciencedirect.com/science/article/pii/`

S0377027312003435 doi: https://doi.org/10.1016/j.jvolgeores.2012.11.013
Clarke, J., Adam, L., & van Wijk, K. (2021). Lp or vt signals? how intrinsic attenuation influences volcano seismic signatures constrained by whakaari volcano parameters [Journal Article]. *Journal of Volcanology and Geothermal Research*, 107337. Retrieved from https://www.sciencedirect.com/science/article/pii/S0377027321001669 doi: https://doi.org/10.1016/j.jvolgeores.2021.107337
Coté, D. M., Belachew, M., Quillen, A. C., Ebinger, C. J., Keir, D., Ayele, A., & Wright, T. (2010). Low-frequency hybrid earthquakes near a magma chamber in afar: Quantifying path effects [Journal Article]. *Bulletin of the Seismological Society of America*, *100*(5A), 1892-1903. Retrieved from https://doi.org/10.1785/0120090111 doi: 10.1785/0120090111
DeGrandpre, K., Wang, T., Lu, Z., & Freymueller, J. T. (2017). Episodic inflation and complex surface deformation of akutan volcano, alaska revealed from gps time-series [Journal Article]. *Journal of Volcanology and Geothermal Research*, *347*, 337-359. doi: 10.1016/j.jvolgeores.2017.10.003
Deichmann, N. (2017). Theoretical basis for the observed break in ml/mw scaling between small and large earthquakes [Journal Article]. *Bulletin of the Seismological Society of America*, *107*, 505-520.
Einarsson, P. (2018). Short-term seismic precursors to icelandic eruptions 1973–2014 [Journal Article]. *Frontiers in Earth Science*, *6*, 45.
Farrell, J., Husen, S., & Smith, R. B. (2009). Earthquake swarm and b-value characterization of the yellowstone volcano-tectonic system [Journal Article]. *Journal of Volcanology and Geothermal Research*, *188*(1), 260-276. Retrieved from https://www.sciencedirect.com/science/article/pii/S0377027309003266 doi: https://doi.org/10.1016/j.jvolgeores.2009.08.008
Garza-Giron, R., Brodsky, E. E., & Prejean, S. G. (2018). Mainshock-aftershock clustering in volcanic regions [Journal Article]. *Geophysical Research Letters*, *45*(3), 1370-1378. Retrieved from https://agupubs.onlinelibrary.wiley.com/doi/abs/10.1002/2017GL075738 doi: https://doi.org/10.1002/2017GL075738
Gibbons, S. J., & Ringdal, F. (2006). The detection of low magnitude seismic events using array-based waveform correlation [Journal Article]. *Geophysical Journal International*, *165*(1), 149-166. Retrieved from https://doi.org/10.1111/j.1365-246X.2006.02865.x doi: 10.1111/j.1365-246X.2006.02865.x
Gualandi, A., Nichele, C., Serpelloni, E., Chiaraluce, L., Anderlini, L., Latorre, D., ... Avouac, J.-P. (2017). Aseismic deformation associated with an earthquake swarm in the northern apennines (italy) [Journal Article]. *Geophysical Research Letters*, *44*(15), 7706-7714. Retrieved from https://agupubs.onlinelibrary.wiley.com/doi/abs/10.1002/2017GL073687 doi: https://doi.org/10.1002/2017GL073687
Harlow, D. H., Power, J. A., Laguerta, E. P., Ambubuyog, G., White, R. A., & Hoblitt, R. P. (1996). Precursory seismicity and forecasting of the june 15, 1991, eruption of mount pinatubo [Journal Article]. *Fire and Mud: eruptions and lahars of Mount Pinatubo, Philippines*, 223-247.
Hatch, R. L., Abercrombie, R. E., Ruhl, C. J., & Smith, K. D. (2020). Evidence of aseismic and fluid-driven processes in a small complex seismic swarm near virginia city, nevada [Journal Article]. *Geophysical Research Letters*, *47*(4), e2019GL085477. Retrieved from https://agupubs.onlinelibrary.wiley.com/doi/abs/10.1029/2019GL085477 doi: https://doi.org/10.1029/2019GL085477
Hensch, M., Riedel, C., Reinhardt, J., & Dahm, T. (2008). Hypocenter migration of fluid-induced earthquake swarms in the tjörnes fracture zone (north iceland) [Journal Article]. *Tectonophysics*, *447*(1), 80-94. Retrieved from https://www.sciencedirect.com/science/article/pii/S0040195107003770 doi:

https://doi.org/10.1016/j.tecto.2006.07.015
Hotovec-Ellis, A. J., Shelly, D. R., Hill, D. P., Pitt, A. M., Dawson, P. B., & Chouet, B. A. (2018). Deep fluid pathways beneath mammoth mountain, california, illuminated by migrating earthquake swarms [Journal Article]. *Sci Adv*, *4*(8), eaat5258. Retrieved from `https://www.ncbi.nlm.nih.gov/pubmed/30116785` doi: 10.1126/sciadv.aat5258
Igarashi, T., Matsuzawa, T., & Hasegawa, A. (2003). Repeating earthquakes and interplate aseismic slip in the northeastern japan subduction zone [Journal Article]. *Journal of Geophysical Research: Solid Earth*, *108*(B5). Retrieved from `https://agupubs.onlinelibrary.wiley.com/doi/abs/10.1029/2002JB001920` doi: https://doi.org/10.1029/2002JB001920
Ji, K. H., & Herring, T. A. (2011). Transient signal detection using gps measurements: Transient inflation at akutan volcano, alaska, during early 2008 [Journal Article]. *Geophysical Research Letters*, *38*(6), n/a-n/a. doi: 10.1029/2011gl046904
Ji, K. H., Yun, S.-H., & Rim, H. (2017). Episodic inflation events at akutan volcano, alaska, during 2005-2017 [Journal Article]. *Geophysical Research Letters*, *44*(16), 8268-8275. doi: 10.1002/2017gl074626
Kanamori, H., & Brodsky, E. E. (2004). The physics of earthquakes [Journal Article]. *Reports on Progress in Physics*, *67*(8), 1429.
Kurihara, R., & Obara, K. (2021). Spatiotemporal characteristics of relocated deep low-frequency earthquakes beneath 52 volcanic regions in japan over an analysis period of 14 years and 9 months [Journal Article]. *Journal of Geophysical Research: Solid Earth*, *126*(10), e2021JB022173. Retrieved from `https://agupubs.onlinelibrary.wiley.com/doi/abs/10.1029/2021JB022173` doi: https://doi.org/10.1029/2021JB022173
Kurihara, R., Obara, K., Takeo, A., & Tanaka, Y. (2019). Deep low-frequency earthquakes associated with the eruptions of shinmoe-dake in kirishimavolcanoes [Journal Article]. *Journal of Geophysical Research: Solid Earth*, *124*(12), 13079-13095. Retrieved from `https://doi.org/10.1029/2019JB018032` doi: https://doi.org/10.1029/2019JB018032
Lanza, F., Roman, D. C., Power, J. A., Thurber, C. H., & Hudson, T. (2022). Complex magmatic-tectonic interactions during the 2020 makushin volcano, alaska, earthquake swarm [Journal Article]. *Earth and Planetary Science Letters*, *587*, 117538. Retrieved from `https://www.sciencedirect.com/science/article/pii/S0012821X22001741` doi: https://doi.org/10.1016/j.epsl.2022.117538
Lu, Z., & Dzurisin, D. (2014). Insar imaging of aleutian volcanoes [Book Section]. In *Insar imaging of aleutian volcanoes* (p. 87-345). Springer.
Lu, Z., Wicks, C., Power, J. A., & Dzurisin, D. (2000). Ground deformation associated with the march 1996 earthquake swarm at akutan volcano, alaska, revealed by satellite radar interferometry [Journal Article]. *Journal of Geophysical Research: Solid Earth*, *105*(B9), 21483-21495. doi: 10.1029/2000jb900200
Marsan, D., & Lengliné, O. (2008). Extending earthquakes' reach through cascading [Journal Article]. *Science*, *319*(5866), 1076-1079. Retrieved from `https://www.science.org/doi/abs/10.1126/science.1148783` doi: doi:10.1126/science.1148783
Matoza, R. S., Shearer, P. M., & Okubo, P. G. (2014). High-precision relocation of long-period events beneath the summit region of kılauea volcano, hawai'i, from 1986 to 2009 [Journal Article]. *Geophysical Research Letters*, *41*(10), 3413-3421. doi: 10.1002/2014gl059819
Melnik, O., Lyakhovsky, V., Shapiro, N. M., Galina, N., & Bergal-Kuvikas, O. (2020). Deep long period volcanic earthquakes generated by degassing of volatile-rich basaltic magmas [Journal Article]. *Nat Commun*, *11*(1), 3918. Retrieved from `https://www.ncbi.nlm.nih.gov/pubmed/32764570` doi: 10.1038/s41467-020-17759-4

Miller, T. P., McGimsey, R., Richter, D., Riehle, J., Nye, C., Yount, M., & Dumoulin, J. A. (1998). *Catalog of the historically active volcanoes of alaska* [Book]. United States Department of the Interior, United States Geological Survey.

Mogi, K. (1963). Some discussions on aftershocks, foreshocks and earthquake swarms: the fracture of a semi-infinite body caused by an inner stress origin and its relation to the earthquake phenomena (third paper) [Journal Article]. *= Bulletin of the Earthquake Research Institute, University of Tokyo*, *41*(3), 615-658.

Munafò, I., Malagnini, L., & Chiaraluce, L. (2016). On the relationship between mw and ml for small earthquakes [Journal Article]. *Bulletin of the Seismological Society of America*, *106*(5), 2402-2408. Retrieved from `https://doi.org/10.1785/0120160130` doi: 10.1785/0120160130

Nakata, J. S., & Okubo, P. G. (2010). Hawaiian volcano observatory seismic data, january to march 2009 [Journal Article]. *US Geological Survey Open-File Report*, *1079*.

Nishikawa, T., & Ide, S. (2017). Detection of earthquake swarms at subduction zones globally: Insights into tectonic controls on swarm activity [Journal Article]. *Journal of Geophysical Research: Solid Earth*, *122*(7), 5325-5343. Retrieved from `https://agupubs.onlinelibrary.wiley.com/doi/abs/10.1002/2017JB014188` doi: https://doi.org/10.1002/2017JB014188

Nishikawa, T., & Ide, S. (2018). Recurring slow slip events and earthquake nucleation in the source region of the m 7 ibaraki-oki earthquakes revealed by earthquake swarm and foreshock activity [Journal Article]. *Journal of Geophysical Research: Solid Earth*, *123*(9), 7950-7968. Retrieved from `https://doi.org/10.1029/2018JB015642` doi: https://doi.org/10.1029/2018JB015642

Oikawa, G., Aso, N., & Nakajima, J. (2019). Focal mechanisms of deep low-frequency earthquakes beneath zao volcano, northeast japan, and relationship to the 2011 tohoku earthquake [Journal Article]. *Geophysical Research Letters*, *46*(13), 7361-7370. Retrieved from `https://agupubs.onlinelibrary.wiley.com/doi/abs/10.1029/2019GL082577` doi: https://doi.org/10.1029/2019GL082577

Okubo, P. G., & Wolfe, C. J. (2008). Swarms of similar long-period earthquakes in the mantle beneath mauna loa volcano [Journal Article]. *Journal of Volcanology and Geothermal Research*, *178*(4), 787-794. doi: 10.1016/j.jvolgeores.2008.09.007

Peng, W., Marsan, D., Chen, K. H., & Pathier, E. (2021). Earthquake swarms in taiwan: A composite declustering method for detection and their spatial characteristics [Journal Article]. *Earth and Planetary Science Letters*, *574*, 117160. Retrieved from `https://www.sciencedirect.com/science/article/pii/S0012821X21004155` doi: https://doi.org/10.1016/j.epsl.2021.117160

Pesicek, J. D., Wellik, J. J., Prejean, S. G., & Ogburn, S. E. (2018). Prevalence of seismic rate anomalies preceding volcanic eruptions in alaska [Journal Article]. *Frontiers in Earth Science*, *6*(100). Retrieved from `https://www.frontiersin.org/article/10.3389/feart.2018.00100` doi: 10.3389/feart.2018.00100

Pitt, A. M. (2002). Midcrustal, long-period earthquakes beneath northern california volcanic areas [Journal Article].

Power, J. A., Friberg, P. A., Haney, M. M., Parker, T., Stihler, S. D., & Dixon, J. P. (2019). *A unified catalog of earthquake hypocenters and magnitudes at volcanoes in alaska—1989 to 2018* (Report No. 2019-5037). Retrieved from `http://pubs.er.usgs.gov/publication/sir20195037` doi: 10.3133/sir20195037

Power, J. A., Stihler, S. D., Chouet, B. A., Haney, M. M., & Ketner, D. M. (2013). Seismic observations of redoubt volcano, alaska — 1989–2010 and a conceptual model of the redoubt magmatic system [Journal Article]. *Journal of Volcanology and Geothermal Research*, *259*, 31-44. Retrieved from https://www.sciencedirect.com/science/article/pii/S0377027312003009 doi: https://doi.org/10.1016/j.jvolgeores.2012.09.014

Power, J. A., Stihler, S. D., White, R. A., & Moran, S. C. (2004). Observations of deep long-period (dlp) seismic events beneath aleutian arc volcanoes; 1989–2002 [Journal Article]. *Journal of Volcanology and Geothermal Research*, *138*(3-4), 243-266. doi: 10.1016/j.jvolgeores.2004.07.005

Power, J. A., Villaseñor, A., & Benz, H. M. (1998). Seismic image of the mount spurr magmatic system [Journal Article]. *Bulletin of Volcanology*, *60*(1), 27-37. Retrieved from https://doi.org/10.1007/s004450050214 doi: 10.1007/s004450050214

Roland, E., & McGuire, J. J. (2009). Earthquake swarms on transform faults [Journal Article]. *Geophysical Journal International*, *178*(3), 1677-1690. Retrieved from https://doi.org/10.1111/j.1365-246X.2009.04214.x doi: 10.1111/j.1365-246X.2009.04214.x

Roman, D. C., & Cashman, K. V. (2006). The origin of volcano-tectonic earthquake swarms [Journal Article]. *Geology*, *34*(6), 457-460. Retrieved from https://doi.org/10.1130/G22269.1 doi: 10.1130/g22269.1

Ross, Z. E., & Cochran, E. S. (2021). Evidence for latent crustal fluid injection transients in southern california from long-duration earthquake swarms [Journal Article]. *Geophysical Research Letters*, *48*(12), e2021GL092465. Retrieved from https://agupubs.onlinelibrary.wiley.com/doi/abs/10.1029/2021GL092465 doi: https://doi.org/10.1029/2021GL092465

Saccorotti, G., & Lokmer, I. (2021). Chapter 2 - a review of seismic methods for monitoring and understanding active volcanoes [Book Section]. In P. Papale (Ed.), *Forecasting and planning for volcanic hazards, risks, and disasters* (Vol. 2, p. 25-73). Elsevier. Retrieved from https://www.sciencedirect.com/science/article/pii/B9780128180822000020 doi: https://doi.org/10.1016/B978-0-12-818082-2.00002-0

Schaff, D. P. (2008). Semiempirical statistics of correlation-detector performance [Journal Article]. *Bulletin of the Seismological Society of America*, *98*(3), 1495-1507.

Shelly, D. R., Ellsworth, W. L., & Hill, D. P. (2016). Fluid-faulting evolution in high definition: Connecting fault structure and frequency-magnitude variations during the 2014 long valley caldera, california, earthquake swarm [Journal Article]. *Journal of Geophysical Research: Solid Earth*, *121*(3), 1776-1795. Retrieved from https://agupubs.onlinelibrary.wiley.com/doi/abs/10.1002/2015JB012719 doi: https://doi.org/10.1002/2015JB012719

Shelly, D. R., Hill, D. P., Massin, F., Farrell, J., Smith, R. B., & Taira, T. (2013). A fluid-driven earthquake swarm on the margin of the yellowstone caldera [Journal Article]. *Journal of Geophysical Research: Solid Earth*, *118*(9), 4872-4886. Retrieved from https://agupubs.onlinelibrary.wiley.com/doi/abs/10.1002/jgrb.50362 doi: https://doi.org/10.1002/jgrb.50362

Syracuse, E. M., Maceira, M., Zhang, H., & Thurber, C. H. (2015). Seismicity and structure of akutan and makushin volcanoes, alaska, using joint body and surface wave tomography [Journal Article]. *Journal of Geophysical Research: Solid Earth*, *120*(2), 1036-1052. doi: 10.1002/2014jb011616

Thelen, W. A., Matoza, R. S., & Hotovec-Ellis, A. J. (2022). Trends in volcano seismology: 2010 to 2020 and beyond [Journal Article]. *Bulletin of Volcanology*, *84*(3), 26. Retrieved from https://doi.org/10.1007/s00445-022-01530-2 doi: 10.1007/s00445-022-01530-2

Traversa, P., & Grasso, J.-R. (2010). How is volcano seismicity different from tectonic seismicity? [Journal Article]. *Bulletin of the Seismological Society of America*, *100*(4), 1755-1769. Retrieved from https://doi.org/10.1785/

0120090214 doi: 10.1785/0120090214

Ukawa, M., & Ohtake, M. (1987). A monochromatic earthquake suggesting deep-seated magmatic activity beneath the izu-ooshima volcano, japan [Journal Article]. *Journal of Geophysical Research: Solid Earth*, *92*(B12), 12649-12663.

van Wijk, K., Chamberlain, C. J., Lecocq, T., & Van Noten, K. (2021). Seismic monitoring of the auckland volcanic field during new zealand's covid-19 lockdown [Journal Article]. *Solid Earth*, *12*(2), 363-373. Retrieved from https://se.copernicus.org/articles/12/363/2021/ doi: 10.5194/se-12-363-2021

Vidale, J. E., Boyle, K. L., & Shearer, P. M. (2006). Crustal earthquake bursts in california and japan: Their patterns and relation to volcanoes [Journal Article]. *Geophysical Research Letters*, *33*(20). Retrieved from https://agupubs.onlinelibrary.wiley.com/doi/abs/10.1029/2006GL027723 doi: https://doi.org/10.1029/2006GL027723

Waldhauser, F., & Ellsworth, W. L. (2000). A double-difference earthquake location algorithm: Method and application to the northern hayward fault, california [Journal Article]. *Bulletin of the Seismological Society of America*, *90*(6), 1353-1368. Retrieved from http://pubs.er.usgs.gov/publication/70022170 doi: 10.1785/0120000006

Wang, T., DeGrandpre, K., Lu, Z., & Freymueller, J. T. (2018). Complex surface deformation of akutan volcano, alaska revealed from insar time series [Journal Article]. *International Journal of Applied Earth Observation and Geoinformation*, *64*, 171-180. doi: 10.1016/j.jag.2017.09.001

Warren-Smith, E., Chamberlain, C. J., Lamb, S., & Townend, J. (2017). High-precision analysis of an aftershock sequence using matched-filter detection: The 4 may 2015 ml 6 wanaka earthquake, southern alps, new zealand [Journal Article]. *Seismological Research Letters*, *88*(4), 1065-1077.

Wech, A. G., Thelen, W. A., & Thomas, A. M. (2020). Deep long-period earthquakes generated by second boiling beneath mauna kea volcano [Journal Article]. *Science*, *368*(6492), 775-779. Retrieved from https://science.sciencemag.org/content/sci/368/6492/775.full.pdf doi: 10.1126/science.aba4798

White, R., & McCausland, W. (2016). Volcano-tectonic earthquakes: A new tool for estimating intrusive volumes and forecasting eruptions [Journal Article]. *Journal of Volcanology and Geothermal Research*, *309*, 139-155. Retrieved from https://www.sciencedirect.com/science/article/pii/S0377027315003492 doi: https://doi.org/10.1016/j.jvolgeores.2015.10.020

White, R. A. (1996). Precursory deep long-period earthquakes at mount pinatubo: Spatio-temporal link to a basalt trigger [Journal Article].

Wiemer, S., & Wyss, M. (2000). Minimum magnitude of completeness in earthquake catalogs: Examples from alaska, the western united states, and japan [Journal Article]. *Bulletin of the Seismological Society of America*, *90*(4), 859-869. Retrieved from https://doi.org/10.1785/0119990114 doi: 10.1785/0119990114

Xue, X., Freymueller, J., & Lu, Z. (2020). Modeling the posteruptive deformation at okmok based on the gps and insar time series: Changes in the shallow magma storage system [Journal Article]. *Journal of Geophysical Research: Solid Earth*, *125*(2). doi: 10.1029/2019jb017801

Yukutake, Y., Honda, R., Harada, M., Arai, R., & Matsubara, M. (2015). A magma-hydrothermal system beneath hakone volcano, central japan, revealed by highly resolved velocity structures [Journal Article]. *Journal of Geophysical Research: Solid Earth*, *120*(5), 3293-3308. Retrieved from https://agupubs.onlinelibrary.wiley.com/doi/abs/10.1002/2014JB011856 doi: https://doi.org/10.1002/2014JB011856

Yukutake, Y., Ito, H., Honda, R., Harada, M., Tanada, T., & Yoshida, A. (2011). Fluid-induced swarm earthquake sequence revealed by precisely determined hypocenters and focal mechanisms in the 2009 activity at hakone volcano, japan [Journal Article]. *Journal of Geophysical Research: Solid Earth*, *116*(B4). Retrieved from https://agupubs.onlinelibrary.wiley.com/doi/abs/10.1029/2010JB008036 doi: https://doi.org/10.1029/2010JB008036

Yukutake, Y., Yoshida, K., & Honda, R. (2022). Interaction between aseismic slip and fluid invasion in earthquake swarms revealed by dense geodetic and seismic observations [Journal Article]. *Journal of Geophysical Research: Solid Earth*, *127*(4), e2021JB022933. Retrieved from https://agupubs.onlinelibrary.wiley.com/doi/abs/10.1029/2021JB022933 doi: https://doi.org/10.1029/2021JB022933

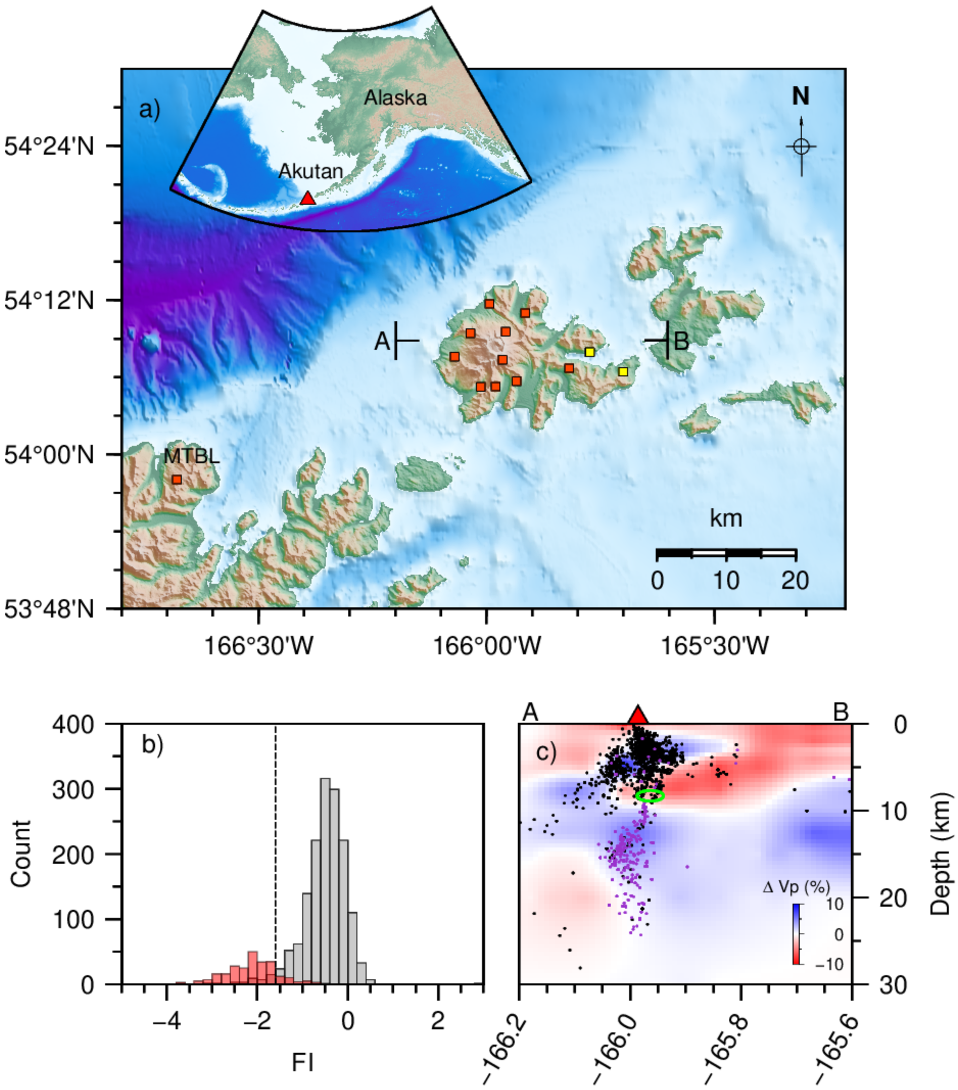

Figure 1. Map view of Akutan volcano along with earthquake distribution. (a) Topography of Akutan Island with cross section from A to B showing location of panel c. Squares represent seismometers used in this study with yellow ones highlighting sites with two co-located seismometers. The inset shows the location of Akutan Volcano in Alaska. (b) FI distribution for 2002-2017 earthquakes with dashed line indicating the threshold of -1.6 used to separate different earthquake types in our study. Colors represent different labels assigned by analysts, i.e. light grey represents VTs while red represents LPs. (c) P wave velocity anomalies across Akutan Volcano (Syracuse et al., 2015) overlain by relocated seismicity during 2005-2017. Earthquakes are classified as VTs and LPs using FI which are represented by black and purple dots respectively. Green ellipse marks the deformation source estimated by DeGrandpre et al. (2017).

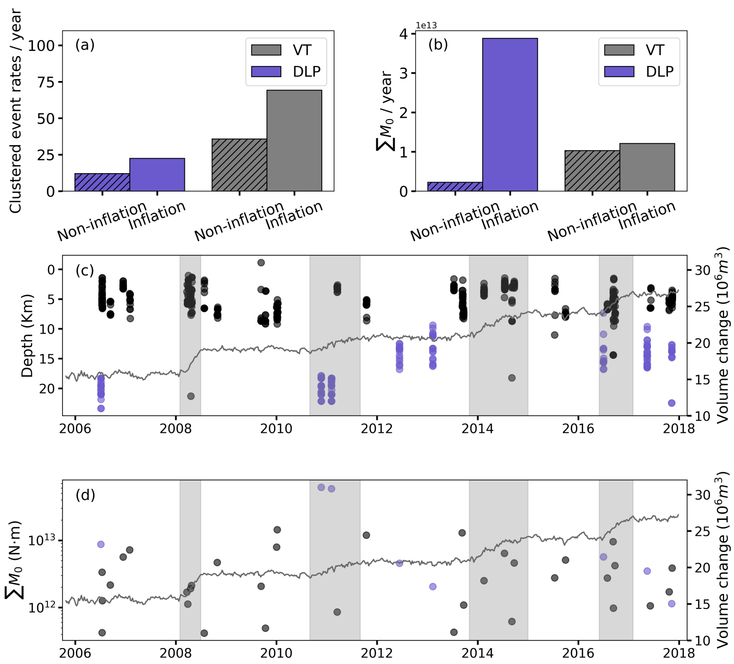

Figure 2. Properties of earthquake swarms at Akutan Volcano from 2005 to 2017. Average occurrence rates (a) and moment release rates (b) of clustered DLPs and VTs during inflation and non-inflation periods. (c) Temporal evolution of earthquake depths. Purple and gray dots represent DLPs and VTs, respectively. Gray curves represent volume changes of deformation source as calculated by Xue et al. (2020). Shaded areas mark inflation episodes. (d) Cumulative moment release of earthquake swarms. Purple and gray dots are DLP and VT swarms, respectively.

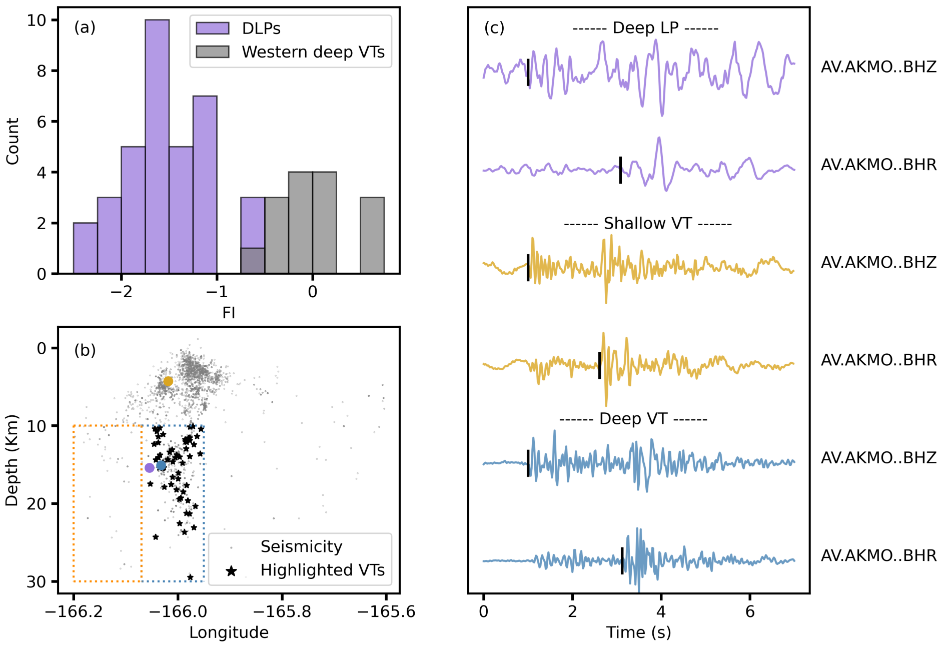

Figure 3. FI analysis on deep VT and DLP earthquakes. (a) FI measured at station MTBL for DLPs and deep VTs to the west of the caldera, with their spatial boundaries outlined by blue and yellow boxes in panel b. (b) Seismicity distribution during 2005-2017 are shown by gray dots. VT detections within the DLP source region are highlighted by black stars. Purple, blue, and yellow dots show locations of DLP, deep and shallow VTs in panel c; (c) Representative waveforms of DLP (purple), deep (blue) and shallow (yellow) VTs recorded by the same local station at vertical and radial channels; black vertical lines indicate phase arrivals.

Supporting Information for "How deep long-period and volcano-tectonic earthquakes relate to magmatic processes at Akutan Volcano"

Zilin SONG[1], Yen Joe TAN[1], Diana C. ROMAN[2]

[1]Earth and Atmospheric Sciences, the Chinese University of Hong Kong, Hong Kong, China

[2]Earth and Planets Laboratory, Carnegie Institution for Science, Washington, DC 20015, USA

Contents of this file

Figures S1 to S11

Additional Supporting Information (Files uploaded separately)

Tables S1 to S2

Introduction Auxiliary material contains eleven figures and two table files.

Corresponding author: Yen Joe TAN, Earth and Atmospheric Sciences, The Chinese University of Hong Kong, Hong Kong, China (yjtan@cuhk.edu.hk)

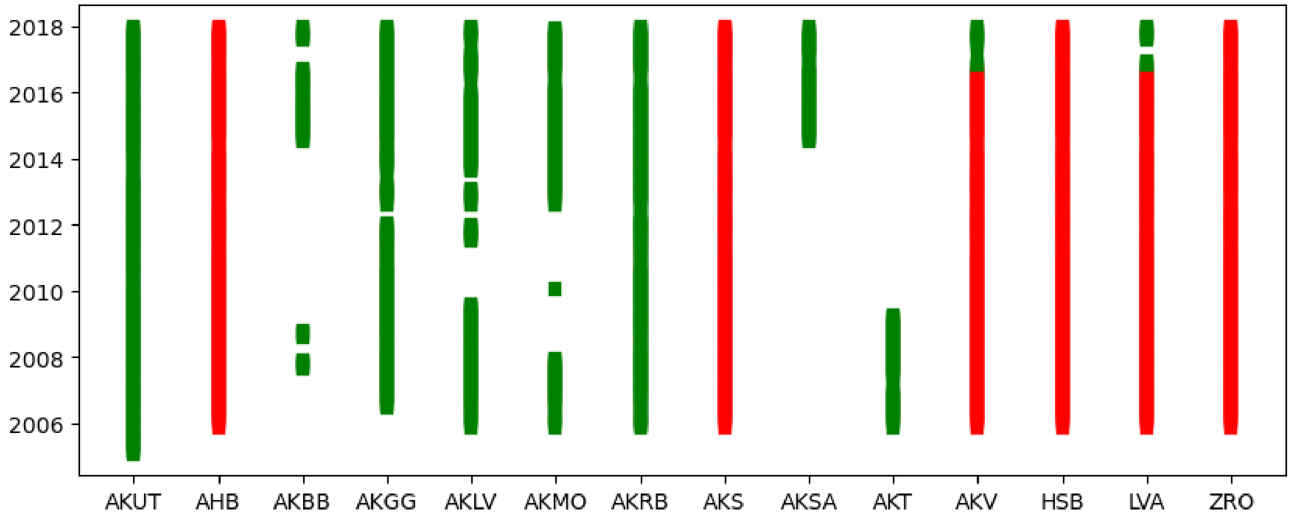

Figure S1. Data availability of stations used for matched filter detections. Red and green lines represent short-period and broad-band seismometers respectively.

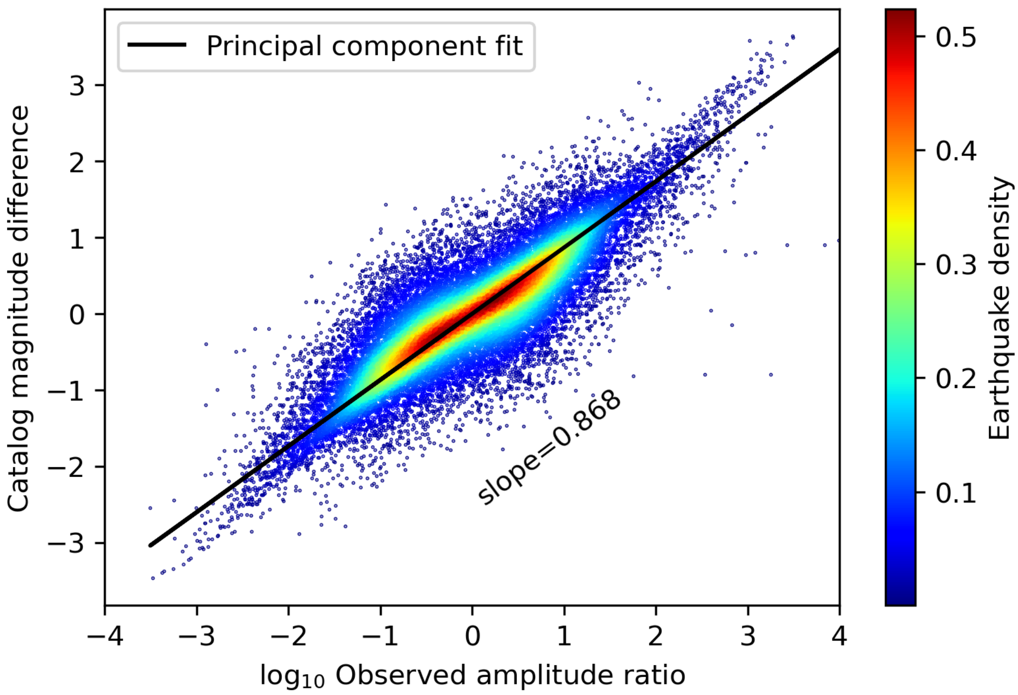

Figure S2. The scaling between observed amplitude ratio and catalog magnitude difference for earthquake templates.

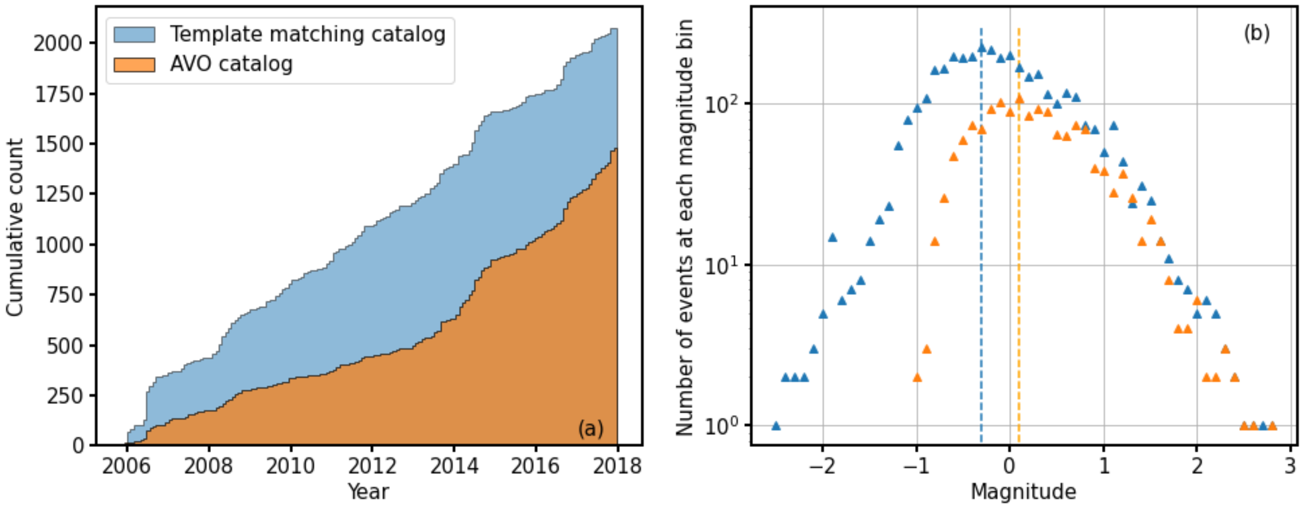

Figure S3. Comparison of earthquake catalogs. (a) Cumulative number of earthquakes in the AVO catalog (Power et al., 2019) and our catalog with template matching detections. (b) Magnitude-frequency distribution of earthquakes at Akutan during 2005-2017. Dashed lines show catalog Mc estimated by max-curvature method (Wiemer & Wyss, 2000).

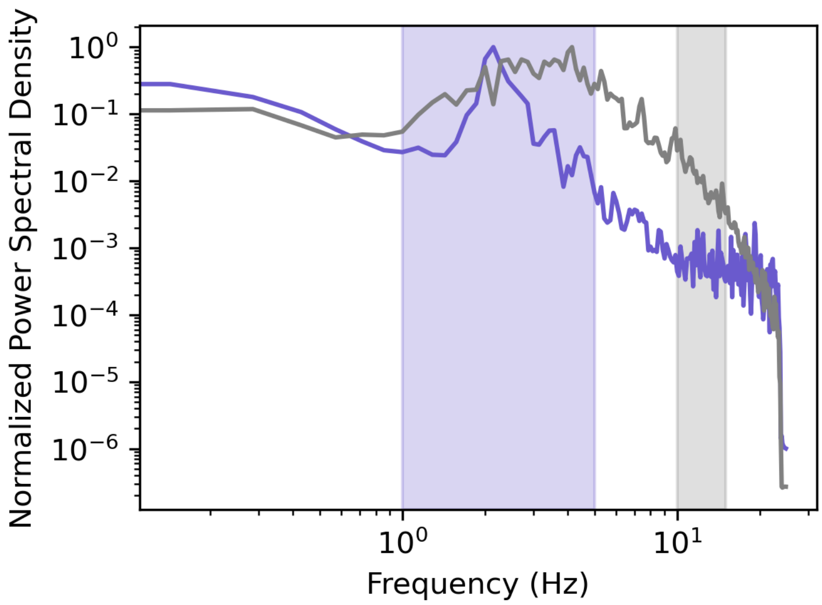

Figure S4. Calibrations for frequency bands selection. Purple and gray lines show stacked spectra for 5 largest LP and VT events during 2005-2017, respectively. The upper and lower frequency bands are highlighted by gray and purple zones.

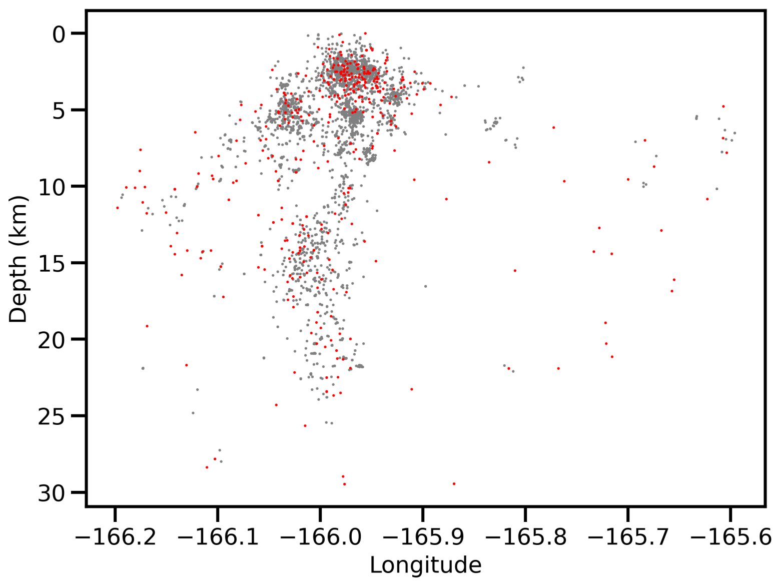

Figure S5. Earthquake distributions at Akutan from 2005-2017. Relocated hypocenters from HypoDD are represented by grey dots. Absolute hypocenters from AVO catalog for earthquakes that were not successfully relocated are depicted by red dots.

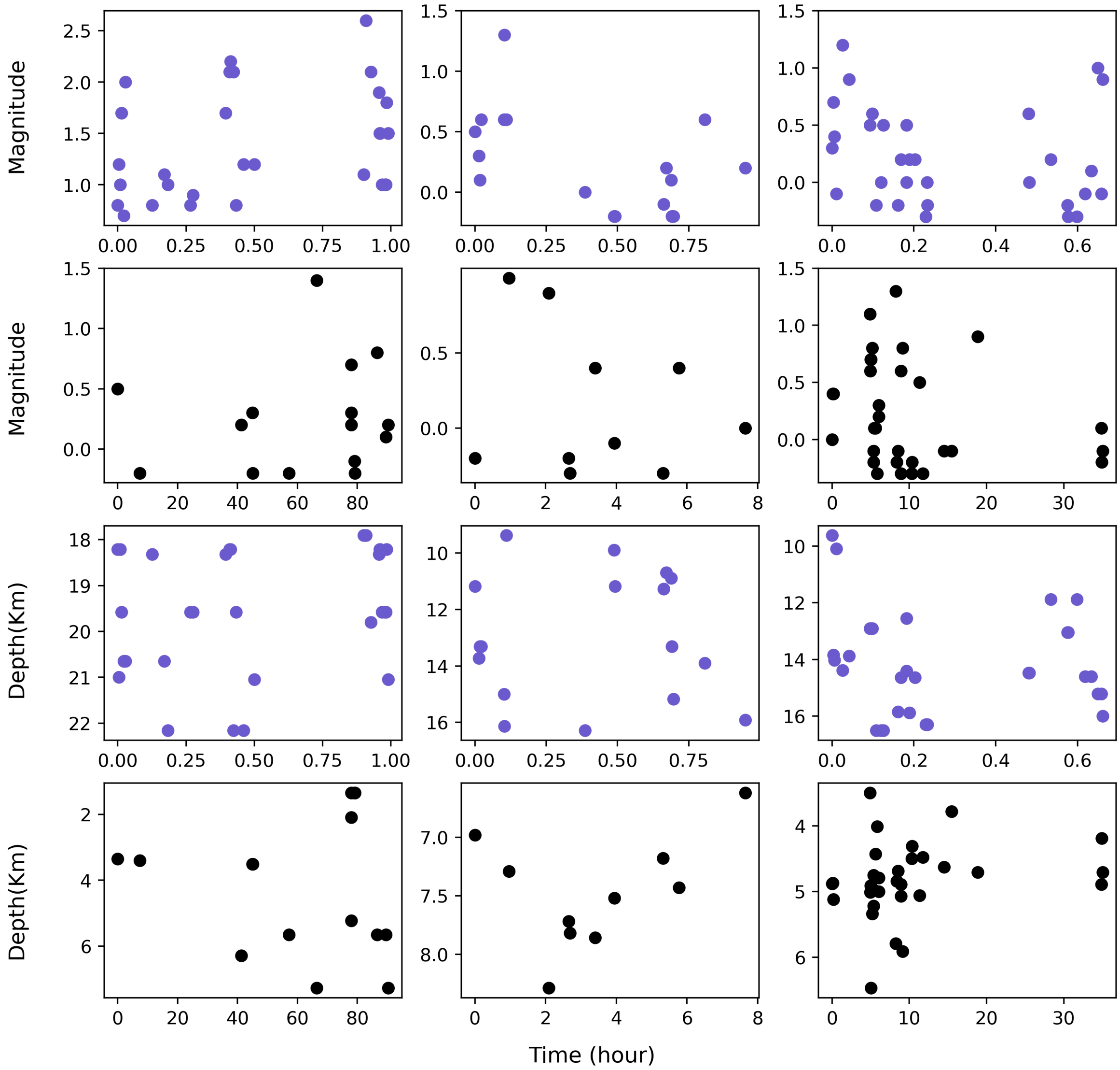

Figure S6. Magnitude-time and depth-time evolution of clustered earthquakes classified as swarms. Purple and black dots represent DLP and VT events respectively.

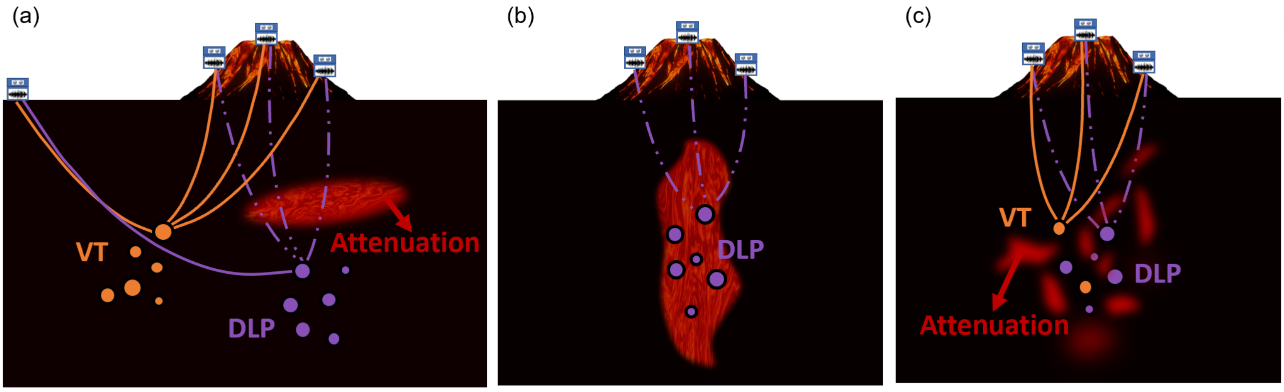

Figure S7. Illustration of three possible path effects: (a) strongly-attenuating region overlying the DLP sources; (b) strongly attenuating region surrounding DLP sources; (c) highly heterogeneous distribution of strongly-attenuating regions around the DLP sources. Solid and dashed lines represent inferred paths with weaker and stronger attenuation effects respectively.

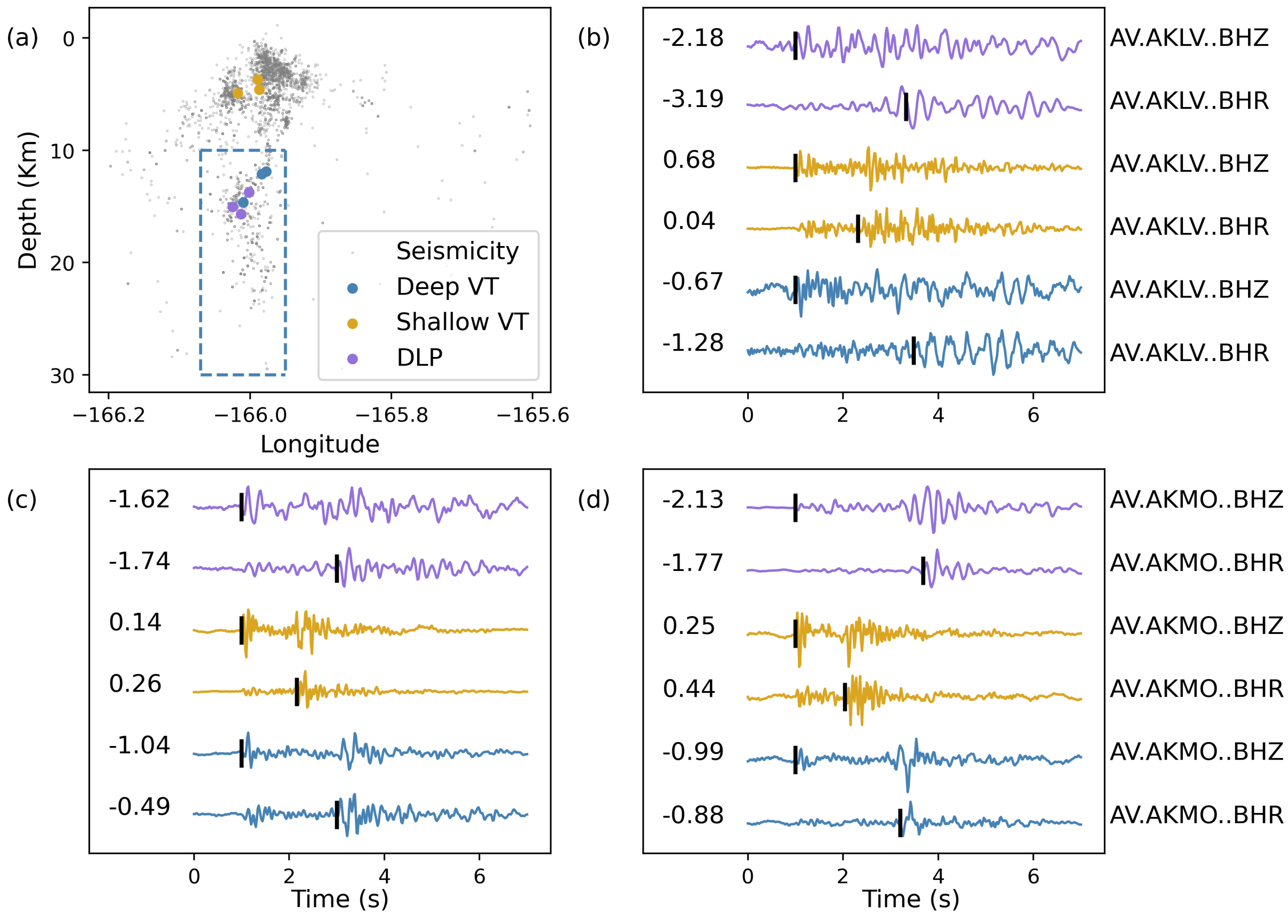

Figure S8. Sample waveforms for earthquakes at Akutan Volcano. (a) Seismicity distributions during 2005-2017 are shown by gray dots. Blue boundaries highlight the DLP source region. Purple, blue, and yellow dots show locations of DLPs, deep and shallow VTs respectively, with corresponding waveforms at station AKMO shown in panel (b), (c), and (d). Black vertical lines in panel (b), (c) and (d) indicate time of manually picked phase arrivals (Power et al., 2019). Numbers listed in panel (b), (c), and (d) show FI of waveforms.

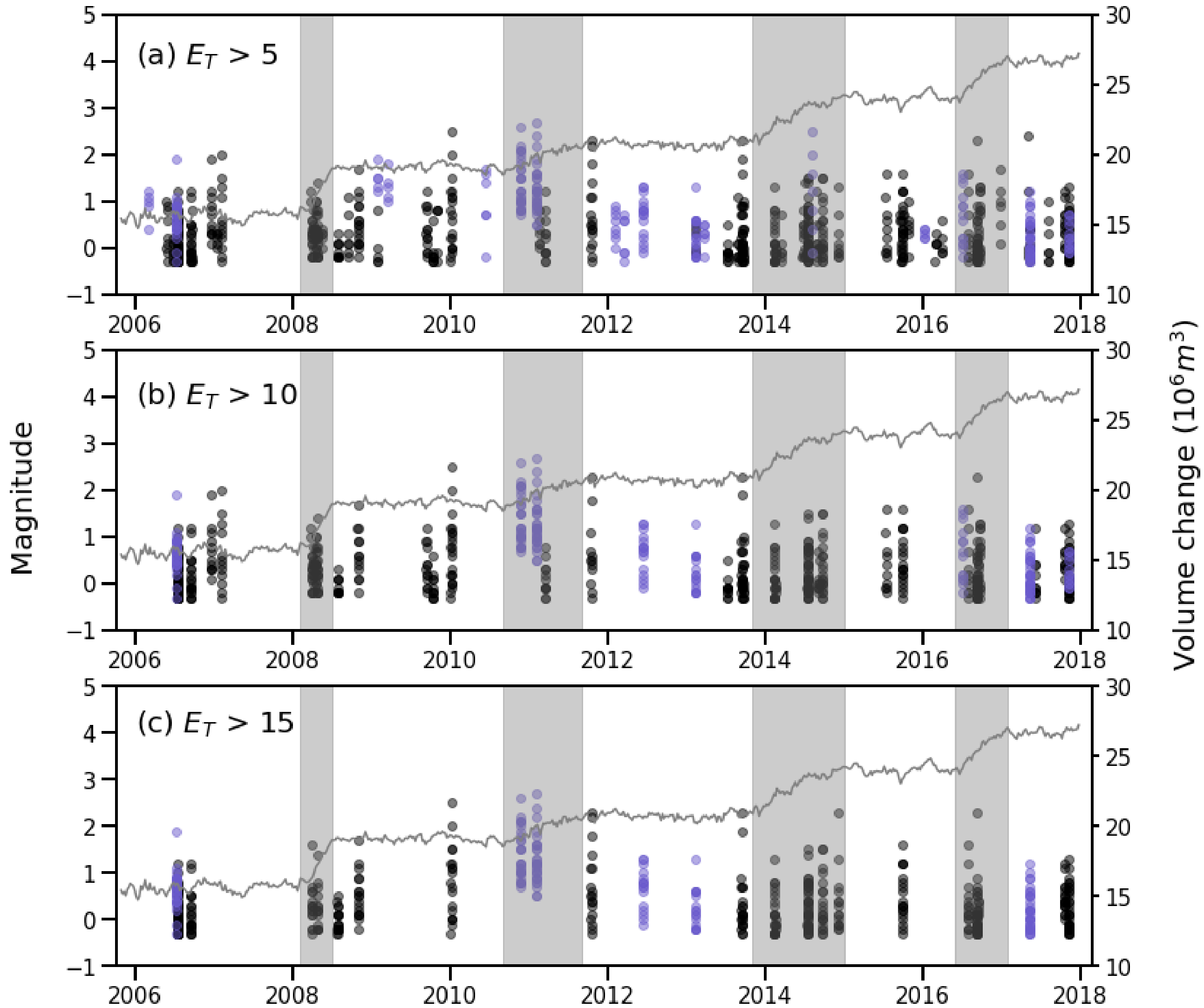

Figure S9. Magnitude-time evolution of clustered seismicity using E_T thresholds of 5 (a), 10 (b), and 15 (c). Black dots represent VTs while purple dots are DLPs. Shaded regions highlight selected inflation episodes. Gray lines show volume changes of deformation source derived by Xue and Freymueller (2020).

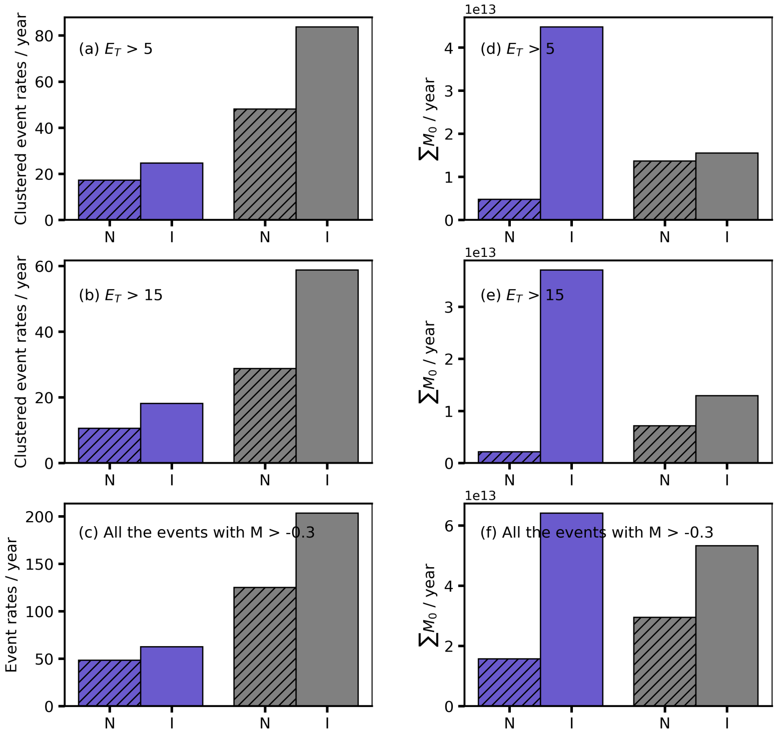

Figure S10. Event rates and moment release rates of clustered DLPs (purple) and VTs (grary) during inflation (I) and non-inflation (N) periods using E_T thresholds of 5 (a, d) and 15 (c, f). In comparison, event rates and moment release rates of all the DLPs and VTs above magnitude completeness are also shown in (c) and (f).

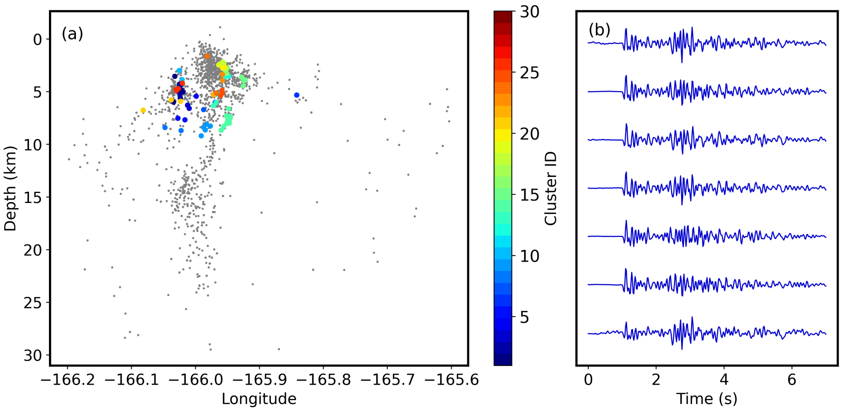

Figure S11. (a) Distribution of seismicity at Akutan are shown by gray dots. Colors are coded by different families of repeating VTs. (b) Sample waveforms in a single repeating VT family at the same local station.